Role of cell polarity dynamics and motility in pattern formation due to contact dependent signalling

Supriya Bajpai
IITB-Monash Research Academy, Mumbai 400076, INDIA
Department of Civil Engineering, Indian Institute of Technology Bombay, Mumbai 400076, INDIA and
Department of Mechanical and Aerospace Engineering,
Monash University, Clayton, VIC 3800, Australia

Ranganathan Prabhakar*
Department of Mechanical and Aerospace Engineering,
Monash University, Clayton, VIC 3800, Australia

Raghunath Chelakkot†
Department of Physics, Indian Institute of Technology Bombay, Mumbai 400076, INDIA

Mandar M. Inamdar‡
Department of Civil Engineering, Indian Institute of Technology Bombay, Mumbai 400076, INDIA

A key challenge in biology is to understand how spatiotemporal patterns and structures arise during the development of an organism. An initial aggregate of spatially uniform cells develops and forms the differentiated structures of a fully developed organism. On the one hand, contact-dependent cell-cell signalling is responsible for generating a large number of complex, self-organized, spatial patterns in the distribution of the signalling molecules. On the other hand, the motility of cells coupled with their polarity can independently lead to collective motion patterns that depend on mechanical parameters influencing tissue deformation, such as cellular elasticity, cell-cell adhesion and active forces generated by actin and myosin dynamics. Although modelling efforts have, thus far, treated cell motility and cell-cell signalling separately, experiments in recent years suggest that these processes could be tightly coupled. Hence, in this paper, we study how the dynamics of cell polarity and migration influence the spatiotemporal patterning of signalling molecules. Such signalling interactions can occur only between cells that are in physical contact, either directly at the junctions of adjacent cells or through cellular protrusional contacts. We present a vertex model which accounts for contact-dependent signalling between adjacent cells and between non-adjacent neighbours through long protrusional contacts that occur along the orientation of cell polarization. We observe a rich variety of spatiotemporal patterns of signalling molecules that is influenced by polarity dynamics of the cells, relative strengths of adjacent and non-adjacent signalling interactions, range of polarized interaction, signalling activation threshold, relative time scales of signalling and polarity orientation, and cell motility. Though our results are developed in the context of Delta-Notch signalling, they are sufficiently general and can be extended to other contact dependent morpho-mechanical dynamics.

I. INTRODUCTION

Morphogenesis is a complex phenomenon in which mechano-chemical pattern formation plays a key role [1]. A large number of self-organising, regular, spatio-temporal patterns in tissues have already been documented. These include, for example, bristle patterns on the *Drosophila notum* [2, 3], spotted skin patterns on pearl danio fish and striped skin patterns on zebrafish [4, 5]. Such spatially differentiated patterns are formed from an aggregate of uniform cells due to cell differentiation process, that acquires a different fate depending on their spatial position [6].

Tissues establish self-organizing chemical patterns by interacting chemically and mechanically [7, 8]. Reaction and diffusion processes involving activators and inhibitors can result in a large variety of the so called Turing patterns in the tissues [9, 10]. Various investigations indicate that a large number of self-organised patterns can also be generated either via short-range signalling interactions mediated by direct cell-cell contact through cell membrane junctions [11] or via long-range signals transmitted through long filapodial protrusions [4, 12]. For example, it is observed that in several multi-cellular organisms, signalling takes place by the lateral inhibition of Delta and Notch, transmembrane molecules, which reside on the surface of multi-cellular organisms such as flies, worms, fish and other vertebrates [13, 14]. Lateral inhibition is a cell interaction process where a cell with a particular fate inhibits the other cells in contact from achieving the same fate. The short-range signalling via lateral inhibition, in which the immediate neighbouring cells in a tissue attain a different fate results in a self-organised checker-board pattern [13]. On the other hand, more complex patterns such as bristle patterns in *Drosophila notum* and stripe patterns in zebrafish can be produced by protrusion-mediated long-range signalling with protrusion directionality and signalling efficiency [15, 16]. Moreover, the patterning dynamics can be speeded up by the inclusion of the mutual inactivation of Delta-Notch along with the dynamics of lateral inhibition [17, 18].

* Prabhakar.Ranganathan@monash.edu
† raghu@phy.iitb.ac.in
‡ minamdar@iitb.ac.in

Coupling between collective cell migration, cell mechanics, and cell-cell signalling is observed in many biological processes such as wound healing, cancer metastasis, branching morphogenesis and embryonic development [19–21]. This coupling is also observed in the case of Delta-Notch signalling. For example, in endothelial cells exhibiting Delta-Notch kinetics, the expression of Dll4 (Delta) is significantly enhanced at the tips of the migrating epithelium during angiogenesis [22]. Also, Delta increase is associated with the motility and spreading of individual keratinocytes [19] and stimulated lamellipodia formation [23]. Furthermore, Delta-induced activation of Notch is linked with the application of mechanical force [24, 25]. Thus there are good indications that spatiotemporal chemical patterns of molecules due to contact-based signalling are associated with cell-cell signalling kinetics, tissue mechanics, cell polarisation dynamics, and cell motility.

The contact-based signalling patterns are interpreted using models generally with a simplifying assumption that the tissue morphology is fixed and does not alter during the patterning process [2, 13, 15, 17, 18]. This assumption may not always be correct since cell migration and cell division can dynamically modify the connectivity among cells. Hence, in order to maintain a regular pattern, the signalling pathway requires some feedback mechanisms to coordinate with cell migration and dynamic tissue topology. In some organisms, such as zebrafish, cell migration plays a vital role in Delta-Notch patterning [26]. Numerical modelling shows that during somitogenesis the synchronization of the segmentation clock is sustained as well as promoted by the randomly moving cells [7], which in turn promote the flow of information across the tissue by cell mixing and destabilizing the regular patterns [8]. In such case, the ratio of time scales of cell migration and cell-cell signalling is crucial for patterning and information transfer between the moving cells [26].

As discussed above, the cell movement characteristics can control the signalling patterns in the tissues. However, the migration pattern of cells in the tissue strongly depends on mechanical properties and cell polarisation dynamics [27]. It is known that the motile cells mechanically interact via elastic forces, contractile forces, cell-cell adhesive forces as well as active forces [28, 29]. The tissue shows a transition from solid to fluid behaviour depending on the cell target shape index, cell motile speed and the polarity dynamics the cells [27]. The cells can orient randomly or exhibit polar alignment and move collectively depending on the persistence time of cell tracks and the local orientation order between them [30, 31]. For example, collective motion with velocity or polar alignment between cells shows the presence of highly dynamic, large-scale moving structures which shows a lane-like or band-like movement of cells in a tissue [32]. Hence it is important to understand the connection between signalling patterns and cell polarisation and migration dynamics.

Although some of existing theoretical models investigate the potential mechanisms that could result in a variety of patterns due to contact-based signalling, to the best of our knowledge, there are no theoretical studies yet that attempt to include the role of tissue mechanics, cell polarisation dynamics, and cell motility influencing them. However, as discussed above, these factors are expected to be important in dictating orientation, range and topology of cellular contacts in the tissue and hence could be critical for the origin and maintenance of the chemical patterns. To test the influence of above mentioned factors in the patterns formed by signalling molecules, we study the system using the well-established vertex model, with several crucial additions. First, we overlay the lateral inhibition based signalling kinetics to the vertex model. We consider both short-ranged as well as long-ranged signalling kinetics, to account for junctional and protrusional contacts [2, 13, 15]. We also study the effect of the activation threshold for long-range signalling on the chemical patterns. Second, we couple the orientation of protrusional contacts with the underlying cell polarities and study the effect of polarisation dynamics on the generated patterns. We specifically look at two cases of polarity dynamics: (i) random rotational diffusion and (ii) polarity alignment with the nearest neighbors. Finally, in addition to cell-signalling, for every cell, we also include cell motility that is oriented along cell polarity and investigate the role of cell migration and tissue mechanics on the resulting signalling patterns due to dynamically evolving cell-cell contacts.

Based on these new additions to the model, in addition to the standard checker-board patterns for signalling molecules, we obtain a large number of intricate patterns ranging from well-defined spotted motifs to diffuse patterns. Moreover, for neighbour aligned polarity dynamics, we see striped patterns of signalling molecules. Upon addition of motility, interestingly, we find that the patterns in signalling molecules maintained, but the cellular structure keeps dynamically shifting in space. We systematically quantify the spatio-temporal characteristics of the chemical patterns by obtaining number of clusters, cluster size distribution and cluster anisotropy of the signalling molecules, as well as dynamic correlation function. Overall, we show that the dynamics of cell polarity and cell motility greatly influences the richness of molecular patterns arising from contact-based signalling.

II. METHODS AND MODEL

In our paper, the mechanics of the tissue is implemented using a vertex model [27–29], in which the tissue is represented as a monolayer formed of polygonal cells having vertices and edges. The mechanical forces within the tissue arise from area elasticity and boundary contractility of individual cells and the forces at cell-cell contacts from acto-myosin contractility and E-cadherin adhesivity. The mechanical contribution from these sources can be expressed using a

work function of the form,

$$U = \sum_{\alpha=1}^{\mathcal{N}} [K_\alpha (A_\alpha - A_{\alpha,0})^2 + \Gamma_\alpha L_\alpha^2] + \sum_{\text{edges:}\gamma\beta} \Lambda_{\gamma\beta} l_{\gamma\beta}, \tag{1}$$

where, $\mathcal{N}$ is the total number of cells in the monolayer and K_α, A_α, $A_{\alpha,0}$, Γ_α, and L_α are the area stiffness, current area, preferred area, boundary contractility and perimeter, respectively, of cell α. $\Lambda_{\gamma\beta}$ is the contractility of the junction of length $l_{\gamma\beta}$ shared by cells γ and β. The contributions from these different forcing terms is converted in effective force acting on any vertex i as

$$\mathbf{F}_i^{\text{elastic}} = -\frac{\partial U}{\partial \mathbf{r}_i}, \tag{2}$$

where $\mathbf{r}_i$ is the position vector for vertex i. In many epithelial tissues, cells are known to be polarised and in many cases also have self-propelled motility. Hence, in addition to the elastic forces, for a given vertex i, we add a motile force [27, 33] of the form

$$\mathbf{F}_i^{\text{active}} = \eta v_0 \frac{1}{n_i} \sum_\beta \hat{\mathbf{p}}_\beta, \tag{3}$$

where n_i is the number of cells β that contain vertex i, $\hat{\mathbf{p}}_\beta$ is the polarity unit vector for cell β, η is the viscous drag acting on the vertex and v_0 is the motility of a single cell. The total force on vertex i, which is a combination of the elastic and active force, is balanced by the external viscous force. The resulting dynamical equation of evolution for the vertex position is

$$\eta \frac{d\mathbf{r}_i}{dt} = \mathbf{F}_i^{\text{elastic}} + \mathbf{F}_i^{\text{active}}. \tag{4}$$

As is common for vertex models, T1 transitions are also included in our formalism and facilitate fluidisation of the tissue.

We model the polarity of every cell to have a tendency to orient with respect to the director ($\pm\mathbf{p}$) of its nearest neighbors while also undergoing rotational diffusion. This rule can be expressed with the following equation

$$\frac{d\theta_\alpha}{dt} = \xi \sum_\beta \sin 2(\theta_\beta - \theta_\alpha) + \zeta_\alpha, \tag{5}$$

where θ_α denotes the orientation angle of cell polarity, $\hat{\mathbf{p}}_\alpha = \cos\theta_\alpha \hat{\mathbf{e}}_x + \sin\theta_\alpha \hat{\mathbf{e}}_y$. Here, ξ is the strength of the polarity alignment of a given cell α with respect to that of its connected cells β and ζ_α is the rotational noise which follows

$$\langle \zeta_\alpha(t)\zeta_\alpha(t')\rangle = 2D_r\delta(t-t'), \text{ and}$$
$$\langle \zeta_\alpha(t)\rangle = 0. \tag{6}$$

In order to study pattern formation of molecules due to contact-based, cell-cell signalling, we now overlay the signalling kinetics on the mechanical vertex model. As discussed earlier, we use Delta-Notch signalling, which is based on contact based lateral inhibition, as our model system [2, 13, 15]. In our formalism, the Delta-Notch kinetics of the cells is modelled by keeping track of Notch and Delta concentration N_α and D_α, respectively, in each cell α. It is known that while Notch concentration in a given cell α increases with the increase in Delta concentration of the cells in contact, the Delta concentration of that cell decreases with increase in its Notch concentration. This signalling dynamics could mathematically be represented as follows

$$\frac{dN_\alpha}{dt} = R_N \frac{\bar{D}_\alpha^2}{a + \bar{D}_\alpha^2} - \mu N_\alpha, \tag{7a}$$

$$\frac{dD_\alpha}{dt} = R_D \frac{1}{b + N_\alpha^2} - \rho D_\alpha, \tag{7b}$$

where $R_N|\mu$ and $R_D|\rho$ are, respectively, the production | decay rates of Notch and Delta. Here, $\bar{D}_\alpha$ denotes the mean Delta concentration in the cells that are in direct contact with cell α through cell-cell junctions and cellular protrusions. More specifically,

$$\bar{D}_\alpha = \frac{1}{2}[\beta_j \bar{D}_j^\alpha + \beta_p \bar{D}_p^\alpha],$$

where β_j and β_p correspond to the contact weights for nearest neighbor and protrusional contacts, respectively, such that $\beta_j + \beta_p = 1$. We define

$$\bar{D}_j^\alpha = \frac{1}{n_j} \sum_{\gamma \in n_j} D_\gamma \text{ and} \tag{8a}$$

$$\bar{D}_p^\alpha = \frac{1}{n_p} \sum_{\gamma \in n_p} D_\gamma, \tag{8b}$$

where n_j and n_p are the number of cells in contact with cell α, respectively, via cell-cell junctions and protrusions. The nearest neighbors of the cell α constitute n_j. Below we outline the procedure followed to obtain the n_p cells that contact cell α through protrusions.

The coupling between the mechanical vertex model and the signalling kinetics is made by identifying that the protrusions of cells are indicative of polarity and motility of the cells [34, 35]. In that spirit, cell protrusions are modelled by assuming a protrusional length l extending along the orientation of cell polarization, $\hat{\mathbf{p}}_\alpha$ and $-\hat{\mathbf{p}}_\alpha$ [15]. We assume that the cellular protrusions lie in a interval of $[-\Delta\theta, \Delta\theta]$ around the directions $\hat{\mathbf{p}}_\alpha$ and $-\hat{\mathbf{p}}_\alpha$. We choose the protrusion length l of cell protrusion [2]. We assume that signalling takes place when the protrusion of a given cell makes contact with the protrusion of other cells within an annulus of thickness Δl around the protrusion length l of the protrusion. Thus effectively, protrusions of two cells can potentially contact with each other for signalling only if the distance between the centers of the cells is within the interval $[2(l-\Delta l), 2(l+\Delta l)]$ – let us term this as separation criterion. However, the extent of cellular protrusions overlap depends on the relative positions of cell pairs, polarity of each cell and the angular sweep of protrusions $2\Delta\theta$ (Fig. 1). For example, if $\Delta\theta = \pi/2$, then any pair of cells that satisfy the separation criterion will be in large protrusional overlap with each other. Similarly, if $\Delta\theta$ is small, then any

pair of cells satisfying the separation criterion would have relatively small protrusional overlaps, and that too for only certain relative positions and polarity orientations (Figs. 1bc).

The signalling between the contacting cells is believed to have an activation threshold [2] that, for example, could depend on the extent of the overlap [36–38]. The exact protrusional overlap between the pair of cells can be calculated using geometry. However, since in our model we couple the protrusion orientation with the cell polarity which constantly evolves in time (Eq. 5), for computational convenience we use a simpler criteria for overlap that also includes the signalling activation threshold T in a coarse-grained fashion. In our model, we define

$$w^{\alpha\beta} = \max\Big[\frac{1}{2}((\hat{\mathbf{p}}_\alpha\cdot\hat{\mathbf{r}}_{\alpha\beta})^2+(\hat{\mathbf{p}}_\beta\cdot\hat{\mathbf{r}}_{\alpha\beta})^2), \sin^2\Delta\theta\Big]. \quad (9)$$

Only if $w^{\alpha\beta} \geq T$ and the cell separation criterion is satisfied there exists protrusional contact between the cell pair α, β. Here, $\hat{\mathbf{r}}_{\alpha\beta}$ is the unit vector from the center of cell α to the center of cell β (Fig. 1c).

The different parameters used in our model are non-dimensionalised as discussed in Appendix A and shown in Table I.

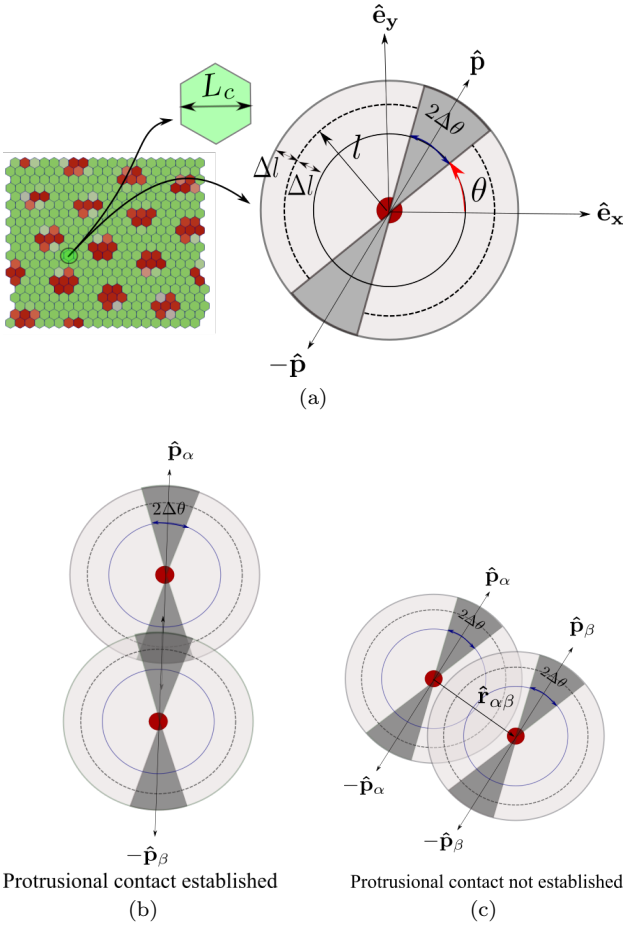

FIG. 1. Schematic showing protrusion along cell polarization and contact interactions with neighbors. (a) Single cell with polarisation $\hat{\mathbf{p}} = \cos\theta\mathbf{e}_x + \sin\theta\mathbf{e}_y$ and protrusions along $\hat{\mathbf{p}}$ and $-\hat{\mathbf{p}}$. Length of protrusions is l and its angular spread is $2\Delta\theta$ around θ and $\theta+\pi$. (b) Cellular protrusions of two cells overlapping each other. Likelihood of contact for two cells is high if their cell polarization vectors are coaxial or the angular range of protrusion is high. (c) Protrusions of two cells that are within range $[2(l-\Delta l), 2(l+\Delta l)]$ of one another but do not touch/overlap.

III. RESULTS

As described in Section II, there are different factors that interact with each other to control the fate of Delta-Notch pattern formation. Some of these are the relative contributions from junctional and protrusional contacts (β_j/β_p), Delta-Notch signalling rates ($\rho \approx \mu \approx R_D \approx R_N$), polarity orientation time-scales ($1/D_r, 1/\xi$), length and overlap margin of protrusions ($l, \Delta l$), angular range of protrusions ($\Delta\theta$), and neighbour exchange time-scales (L_c/v_0), where L_c is the characteristic length scale of the system (Fig. 1a). For example, in the case, when $\Delta\theta$ is large, the contact between any pair of cells only depends on the spacing between the cells. Hence, the pattern formation is expected to be predominantly dictated by the relative time-scales L_c/v_0 over which the cells move away from each other and $1/\rho$. On the other hand, when $\Delta\theta$ is small, even if the spacing between the cells does not change (e.g., when $v_0 \approx 0$) the pattern formation from protrusional contacts should still be influenced by the time-scales for polarity changes $1/D_r$ when compared with the signalling time-scales $1/\rho$. In this section, we systematically explore, how these different chemical and mechanical factors decide the spatio-temporal dynamics of signalling patterns. In Sec. IIIA-C, we study the role of mechanochemical parameters on signalling patterns when cell motility is low. The effect of cell motility on signalling patterns is explicitly investigated in Sec. III D.

A. Role of contact ratio (β_j/β_p) from junctional and protrusion-mediated contacts

The strength of Delta–Notch signalling at junctional and protrusional contacts is captured by β_j and β_p, respectively. The contact ratio β_j/β_p is critical for deciding signalling pattern in this model. When the contact ratio is large $\beta_j/\beta_p \gg 1$ checker board pattern emerges since the signalling is dominated by the junctional contacts as in the classic model by Collier et al. [13] (Fig. 2a) and (Movie 1). On the other hand, consider the case of small contact ratio $\beta_j/\beta_p \ll 1$ with $\Delta\theta = \pi/2$ (Fig. 2b) and (Movie 2). Here, the dominant mode of signalling is through cell protrusions. Moreover, for $\Delta\theta = \pi/2$, the cell-cell signalling is isotropic and occurs for any pair of cells that satisfy the separation criterion. The signalling pattern in this case is similar to the checkerboard pattern observed for large contact ratio. However, the pattern shows a new length scale corresponding to the size of protru-

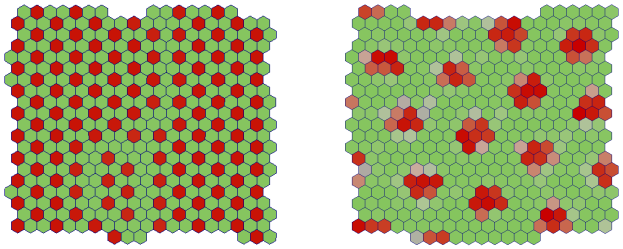

(a) (b)

FIG. 2. Signalling patterns formed by contact mediated signalling via (a) junctional contacts $\beta_j \gg \beta_p$ and (b) protrusional contacts $\beta_p \gg \beta_j$.

sions ($2l \approx 3$ cell-lengths). Thus the nature of pattern formation in contact based signalling is influenced by the relative strengths of junctional and protrusional contacts.

B. Role of angular range of protrusions ($\Delta\theta$) and activation threshold (T)

As discussed in Sec. II, long-range signalling can be achieved by protrusional contacts. As described there, the orientation of protrusion for any cell α is decided by the direction of cell polarization $\pm\hat{\mathrm{p}}_\alpha$. In this sector we consider the case where the cell polarization is governed by the random rotational diffusion only ($\xi = 0$). The signalling dynamics additionally depend on the length and overlap range of protrusion (l, Δl), the angular range of the protrusions $\Delta\theta$ and activation threshold (T). We now systematically study the effect of $\Delta\theta$ and T on signalling patterns by varying only these two while keeping all other model parameters fixed (Fig. 3) and (Movie 2-7). The patterns The protrusions are more polarized if $\Delta\theta$ is smaller and the protrusions are not at all polarized if $\Delta\theta = \pi/2$, ie, the protrusions can grow in all directions. The smaller the $\Delta\theta$, the protrusions are more polarized ie, if $\Delta\theta = 0$ the protrusions are polarized to grow only in the direction of polarization.

We keep $\Delta\theta = \pi/4$ and explore how the steady-state signalling patterns evolve with the activation threshold T. When T is relatively small, we see isolated, ordered patterns of sharp isotropic spots of Delta expression, similar to the ones already discussed in Sec. III A (see Fig. 2b). Upon increase in T, there is an increase in Delta signalling (Eq. 9) that results in reduction of Notch in cells and hence a general increase in Delta levels (Eq. 9). Moreover, the Delta-Delta signalling also gets relatively anisotropic in patches. As a result, the Delta expression patterns start getting less structured, more elongated, and increasingly connected. This effect becomes most pervasive at the largest threshold value.

We now quantify different aspects of Delta patterns that are observed for various combinations of $\Delta\theta$ and T. To get insights into the connectivity of the Delta patches, we compute the median number of Delta clusters and median size (number of Delta cells per cluster) of isolated Delta clusters. We define one cluster of Delta cells as the group of connected cells, each with Delta concentration $D > D_{\mathrm{critical}}$ (see Appendix B). To also get insight into the geometry of these patches, we then quantify their shape ratio (see Appendix C). In Figs. 3g, 3h and 3i, respectively, we represent the median number of clusters, median size of the clusters and their median shape ratio, averaged over space and time, as functions of $\Delta\theta$ and T. By observing these phase-diagrams together we can see that, for lower values of T the Delta expression patterns are isolated in small isotropic clusters (Figs. 3ab). However, upon increase in T, the clusters keep getting smaller in numbers, i.e, larger in size, and become increasingly elongated for lower values of $\Delta\theta$ (Figs. 3cd). For largest values of T, the clusters remain bigger but become more isotropic due to increasing connectivity of Delta regions (Fig. 3ef). For large values of $\Delta\theta$, however, the clusters always remain small and isotropic, as discussed in Sec. III A.

We thus find that a rich array of Delta-Notch patterns are observed due to an interplay between the angular range of protrusions and the threshold for signalling at protrusional contacts and provide an effective way of quantifying their nature.

C. Role of coupling strength ratio (ξ/D_r) on pattern formation

In our model, the dynamics of cell polarity has two components (Eq. 5). The first component tends to align the polarity of any cell with that of its nearest neighbors with rate ξ and attempts to bring about global alignment of polarity in the tissue [32]. The second component D_r brings about rotational diffusion of cell polarity, thus creating an overall disorder in tissue polarity. As studied in the previous section, for the case of polarity alignment rate $\xi = 0$, the cell polarities dictate the local dynamics of protrusional contacts (Eq. 9) and hence the Delta-Notch patterns. However, since ξ influences the global alignment of cell polarity, in this section we study the role of the coupling strength ratio ξ/D_r on Delta-Notch pattern formation.

We fix $T = 0.5, D_r = 0.1, \Delta\theta = \pi/4$ and vary the value of ξ from $0 - 0.25$. The progressively changing patterns for increasing magnitude of ξ/D_r are shown in (Figs. 4a-f) and (Movie 8-13). As expected, when ξ is relatively small, D_r dominates and the cell polarity is spatially disordered, thus resulting in isotropic circular patterns of Delta expression (also see Fig. 3a). However, when ξ becomes comparable to D_r, the spatial disorder of cell polarity decreases and local regions of polarity alignment with an effective direction are created. Since protrusions are oriented along the polarity of cells in our model, the cell-cell contacts predominantly occur along the effective polarity orientation and very little in the perpendicular direction. As a result, the Delta signalling is diminished along the perpendicular direction resulting in reduction of Notch levels along that direction. The lowering of Notch concentration, in turn, results in greater expression of Delta, thus leading to formation of elongated

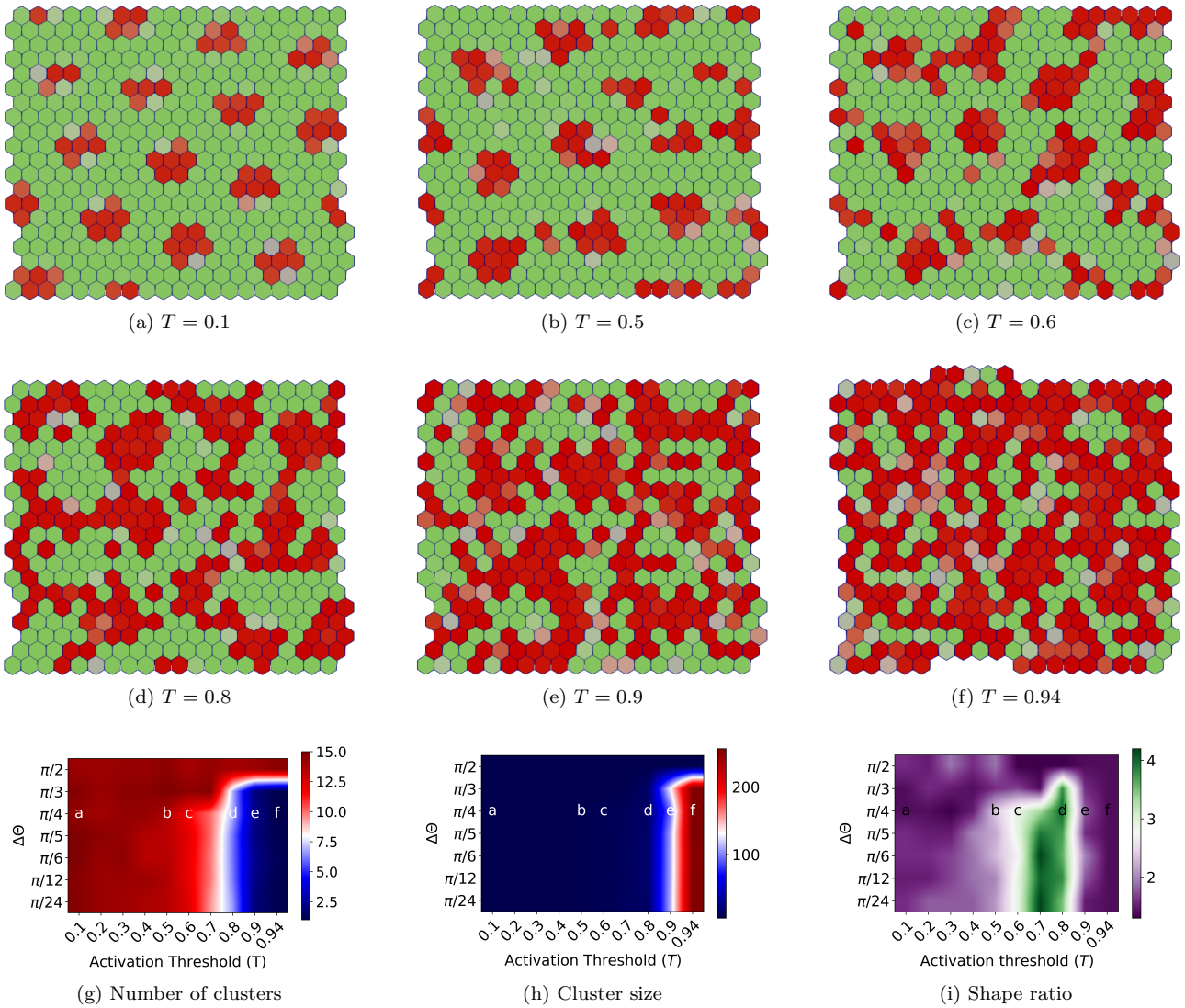

FIG. 3. Role of angular range of protrusions $\Delta\theta$ and activation threshold T on pattern formation. (a-f) Steady-state Delta(red)-Notch(green) patterns obtained with $R_N = R_D = \rho = \mu = 1$, $D_r = 10^{-3}$, ${}^{\beta_j}/_{\beta_p} = 10^{-2}$, $\Delta\theta = \pi/4$, $v_0 = 3.1 \times 10^{-4}$, and $\Lambda = -13.77$, $\xi = 0$ and varying $T \in [0.1, 0.5, 0.6, 0.8, 0.9, 0.94]$. (g,h) Phase diagrams for the median number of clusters and the median cluster size (median number of Delta cells per cluster) in a confluent tissue as a function of $\Delta\theta$ and T. Large value of cluster number with small cluster size indicates many isolated small Delta patches, whereas a small number of clusters with large cluster size indicates connected regions of Delta expression. (i) Phase diagram for the median shape ratio of Delta clusters in a confluent tissue as a function of $\Delta\theta$ and activation threshold T. Lower and higher values of this quantity indicate dominant presence of circular and elongated patches, respectively.

Delta domains. Consequently, we see Delta expression emerging in stripe-like patterns that are oriented perpendicular to the overall direction of cell polarity in the ordered region. In the region with disordered polarity we still observe circular regions of Delta expression. As expected, the thickness of stripes and the diameter of the circular spots are roughly equal to twice the protrusion length ($2l \approx 3$ cell lengths). Upon further increase in ξ, the cell polarities align globally, thus resulting exclusively in stripe-like patterns of Delta expression. However, the presence of D_r leads to modification of the global polarity alignment causing the patterns to reorient over longer time-scales (see Movie 8-13).

As we had done in the previous section, we now quantify the median number of clusters, median cluster size and median shape-ratio of the Delta patterns using phase-diagrams obtained as a function of $\Delta\theta$ and ξ/D_r (Figs. 4g 4hand 4i). As expected, for large values of $\Delta\theta$, we mostly observe patterns of isolated, circular clusters, irrespective of the magnitude of ξ/D_r since the cell protrusional contacts are mostly isotropic. However, for lower values of $\Delta\theta$, an increase in ξ/D_r, which results in cell polarity ordering, leads to the formation of uniformly oriented and continuous Delta stripes.

We thus find that polarity dynamics can have a strong influence on the nature of Delta-Notch signalling patterns.

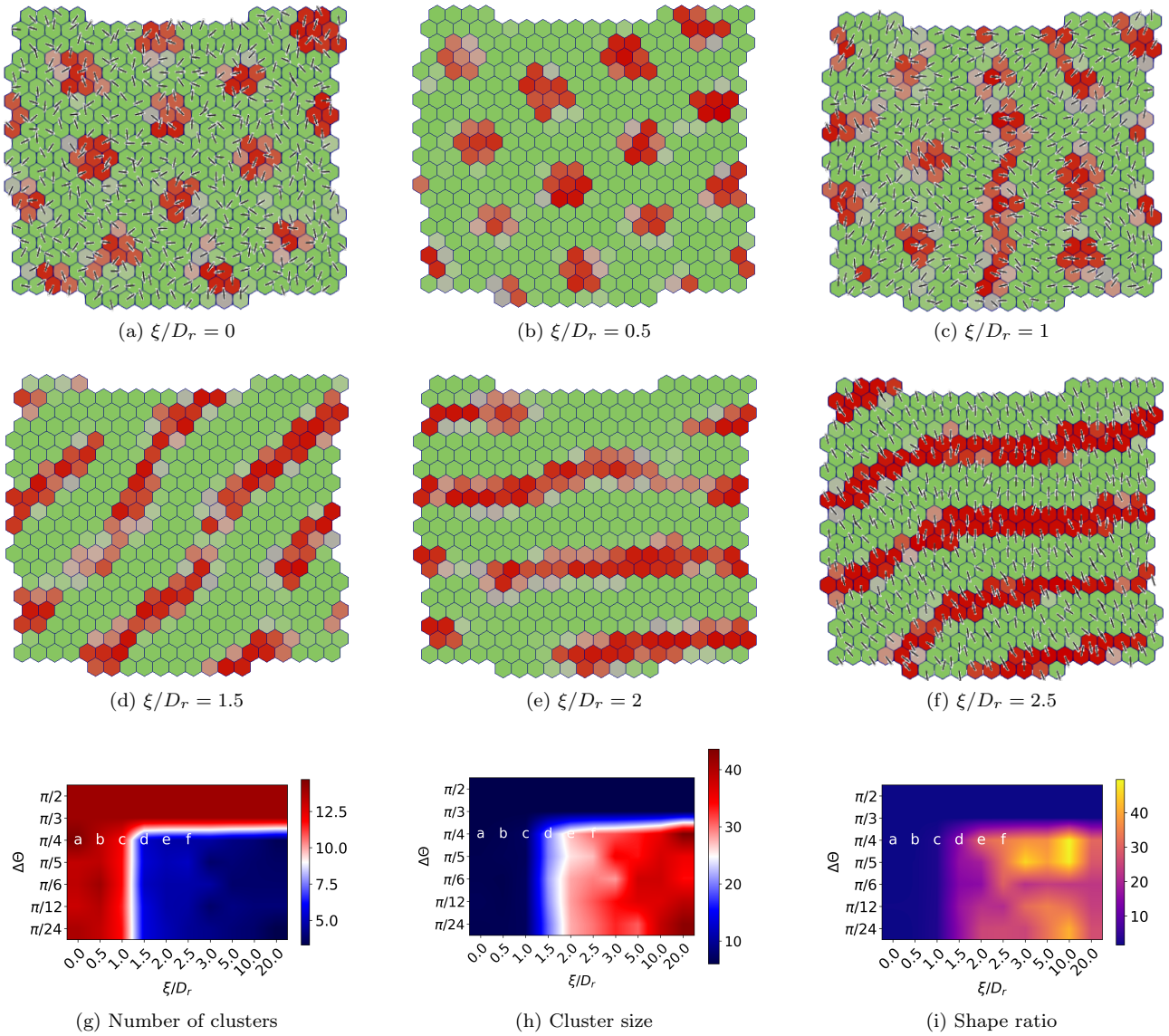

(a) $\xi/D_r = 0$ (b) $\xi/D_r = 0.5$ (c) $\xi/D_r = 1$

(d) $\xi/D_r = 1.5$ (e) $\xi/D_r = 2$ (f) $\xi/D_r = 2.5$

(g) Number of clusters (h) Cluster size (i) Shape ratio

FIG. 4. Screenshots showing the steady state Delta(red)-Notch(green) patterns formed with polarized cells with varying coupling strength ratio (ξ/D_r) and angular range of protrusions ($\Delta\theta$). The fixed parameters are $R_N = R_D = \rho = \mu = 1$, $\Lambda = -13.77$, $D_r = 0.1$, $v_0 = 3.1 \times 10^{-4}$, ${}^{\beta_J}/_{\beta_P} = 0.01$, $T = 0.5$, and $\Delta\theta = \pi/4$. The patterns (a-f) are obtained by varying coupling strength ratio $\xi/D_r \in [0, 0.5, 1.0, 1.5, 2.0, 2.5]$. (g,h) Phase diagrams for the median number of clusters and median cluster size in a confluent tissue as a function $\Delta\theta$ and ξ/D_r. (h) Phase diagram for shape ratio in a confluent tissue as a function of $\Delta\theta$ and ξ/D_r. Large number of Delta clusters with small cluster size and low shape ratio indicate the dominance of isolated circular patterns, wheres low number of clusters with big cluster size and high shape ratio point towards stripe-like patterns.

D. Effect of motility on pattern formation

So far we have studied the role of protrusion spread, signalling threshold and polarity dynamics on the formation of Delta-Notch patterns in tissues. In our model, the polarity dynamics influences the signalling via modification of protrusional contacts. However, cell polarity is also connected with cell migration, which in conjunction with cell shape index can control tissue fluidisation through cell neighbor exchanges and thus influence the signalling pattern. Hence, we provide cells with larger values of motility v_0 and adjust cell line tension Λ such that the cell-shape index $p_0 = -\frac{\Lambda}{4\Gamma\sqrt{A_0}} \approx 3.85 > 3.8$, that is required for tissue fluidisation for $v_0 = 0$ [27, 29, 39]. First, we study the effect of uncorrelated cell movement on pattern formation by fixing $\xi = 0$, $v_0 = 0.31$, and $D_r = 0.001$. If the signalling rates are small, then the neighbor exchanges between the cells are too fast as compared to the signalling time-scales. As a result, we do not observe Delta-Notch patterns as for the static cell network. However, upon increasing the signalling rates by ten-fold, we recover back the circular, isolated patterns seen earlier.

Interestingly, the patterns are now no longer static but keep spatially rearranging. The movement of the Delta patterns mainly depends on the dynamics of the cluster of Delta expressing cells, which in turn is dictated by the collective cell migration patterns that are governed by the underlying tissue mechanics and po-

larity dynamics of individual cells (Figs. 5a-c)(Movie 14,15). In the case where a particular cluster of Delta cells breaks apart, a new group of Delta expressing cells is created by the entry of new cells into a pre-exisiting nuclei of Delta expressing cells. On the other hand, there are cases where the entire group of Delta expressing cells migrates as a whole in which case the Delta patterns also takes the same trajectory as the complete cluster. A combination of these two modes of pattern movements leads to an emergent time-scale of spatial rearrangement of the clusters.

To quantify the spatio-temporal dynamics of these patterns, we calculate the Delta-Delta radial distribution function, $G_d(r,\tau)$ that is given as

$$G_d(r,\tau) = \frac{1}{\kappa\mathcal{N}} \sum_{\alpha} \sum_{\substack{\beta\neq\alpha \\ r<|\mathbf{r}_{\alpha\beta}|\leq r}} \langle D_\alpha(t) D_\beta(t+\tau)\rangle_t, \quad (10)$$

where, κ is the normalization factor given as

$$\frac{1}{\mathcal{N}(\mathcal{N}-1)} \sum_{\alpha} \sum_{\alpha\neq\beta} \langle D_\alpha(t) D_\beta(t+\tau)\rangle_t\rangle$$

The basic idea behind this function is to capture for every cell α at a given time t how much does its Delta expression correlates with the Delta levels of every other cell β that is present within a particular distance $r < |\mathbf{r}_\beta - \mathbf{r}_\alpha| \leq r + \Delta r$ at time $t+\tau$. The plots of $G(r,\tau)$ as a function of r for different time-lags τ are shown in (Fig. 5d). When $\tau = 0$, we see a decaying oscillatory pattern in space that is indicative of periodic Delta expression with the distance between the centers of neighboring Delta region of approximate 5 cells. For increasing values of τ, we see that the shape of $G_d(r,\tau)$ remains invariant, but the amplitude of the function decreases, thus indicating that the patterns are not stationary but diffuse in space. To quantify the rearrangement time-scale of the Delta patterns, we plot the amplitudes of the radial distribution function $G_d(r,\tau)$ corresponding to its first minima $r \approx 2.5$ as a function of time-lag τ (Fig. 5e). After fitting an expression of the form $A + B\exp(-\tau/\mathcal{T})$, the pattern re-arrangement time-scale $\mathcal{T} \approx 90$.

We also study the effect of cell movement on pattern formation when the alignment strength ratio ξ/D_r is relatively high with $\xi = 0.25$, $v_0 = 0.31$, and $D_r = 0.1$. In this case, we see that stripe-like patterns of Delta expression are seen similar to the case when $v_0 = 10^{-4}$. However, the patterns are more dynamic and, as opposed to the formation and breaking of clusters in the case of spot-like patterns when $\xi = 0$, we see that the stripes break and merge to continuously change their alignment.

Thus, we observe that the polarity and motility dynamics of cells, along with tissue mechanics, influence the signalling patterns and hence the spatio-temporal levels of Delta and Notch expression.

IV. DISCUSSION

In this study, we report a rich variety of Delta-Notch patterns that depend on the nature of cell-cell contacts, signalling threshold, polarity dynamics, cell motility and tissue mechanics. The classic model by Collier et al. [13] exhibits checkerboard pattern for Delta-Notch expression. We show that this pattern modifies to a spot-like like pattern due to long-range contacts with essentially a change in the length-scale that arises due to linear protrusion range. However, the modification in the angular range of protrusional contacts elicits local contact anisotropy and hence results in more elongated Delta patterns. We further showed that the signalling threshold is also important in dictating the connectivity of Delta clusters. Moreover, we systematically quantified the nature of these patterns by measuring the number of Delta cells cluster, cluster size and calculating the shape of individual clusters. We see that by changing the polarity dynamics by increasing the signalling ratio ξ/D_r, the cell directors ($\pm\mathbf{p}$) become globally aligned thus leading to the formation of stripe-like patterns. We also observed that when the cells have motility and shape index beyond the fluidisation threshold, the cells can rapidly change their connectivity due to which their signalling contacts are also modified. As a result, the expression patterns for Delta-Notch no longer remain static. Their dynamics is decided by the dynamics of the formation and breaking of Delta clusters, which in turn are governed by the motility patterns of the cells. When the polarity diffusion dominates, we see the formation of moving spot-like patterns, which we systematically quantified using the spatio-temporal radial correlation function for Delta expression. On the other hand, when the polarity alignment term dominates, we saw that stripe-like patterns arise. However, unlike for the static case, the stripes keep modifying their alignment by splitting and then merging with the other stripes – this dynamics being governed by cellular movements.

Lateral inhibition is one of the most ubiquitous mode of signalling, and Delta-Notch signalling is one of the prominent example of this mechanism. Experimentally, the Delta-Notch signalling mechanism has been studied in detail, and its involvement in cell migration, polarity dynamics, and mechanical aspects of morphogenesis is known. Although, there are a few theoretical models that study the Delta-Notch pattern formation in tissues, there are no theoretical studies on how these patterns are themselves influenced by collective cell dynamics. On the other hand, there are a large number of theoretical studies on collective cell migration, especially on the role of cell motility, polarity and cell shape index on tissue unjamming. However, these studies generally do not consider the effect of tissue kinematics on the underlying signalling patterns. In this study, we combined both these aspects and showed how cell level interactions can lead to tissue level formation of a large variety of Delta-Notch patterns. Although in our model, the Delta-Notch pattern is influenced by cellular dynamics, the signalling itself does not influence the cell dynamics. A next step, for example, would be to include the influence on Delta-Notch levels in the cells on motility and cell-cell adhesivity. We finally note that, although our modeling is developed in the context of

TABLE I. The model parameters relative to characteristic length scale $L_c = 1$ (Fig.1a) and characteristic time scale $T_c = 1$

Dimensionless parameters	Parameter values
L_c	1.0
η	1.0
Γ	1.0
$K \equiv \frac{KT_cL_c^2}{\eta}$	1.15
$\Lambda \equiv \frac{\Lambda T_c}{4L_c\eta}$	$[-13.77, -14.32]$
$v_0 \equiv {}^{v_0T_c}/_{L_c\eta}$	$3.1 \times 10^{-4}, 0.31$
$A_0 \equiv A_0/L_c^2$	0.866
$\xi \equiv \xi T_c$	$0 - 2$
$D_r \equiv D_rT_c$	$[0.001, 0.1]$
$D_\alpha \equiv {}^{D_\alpha}/_{D_0}$	$0 - 1$
$N_\alpha \equiv {}^{N_\alpha}/_{N_0}$	$0 - 1$
$R_D \equiv R_DT_c$	$1, 10$
$R_N \equiv R_NT_c$	$1, 10$
$\rho \equiv \rho T_c$	$1, 10$
$\mu \equiv \mu T_c$	$1, 10$
$l \equiv l/L_c$	1.4
$\Delta l \equiv \Delta l/L_c$	0.3
$\Delta\theta \equiv \Delta\theta$	$\pi/24 - \pi/2$
$\Delta t \equiv \Delta t/T_c$	0.01
a	[0.01]
b	[100]
$D_{\text{critical}} \equiv {}^{D_{\text{critical}}}/_{D_0}$	0.5
$\mathcal{N}$	$[400, 1600]$

Delta-Notch signalling, it is sufficiently general, and provides a broad framework to study the role of collective cell dynamics on chemical pattern formation for any contact based signalling.

ACKNOWLEDGEMENTS

MMI and RC acknowledge Industrial Research and Consultancy Centre (IRCC) at IIT Bombay, India, for financial support. RC thanks Science and Engineering Research Board (SERB), India (Project No. ECR/2017/000744, and SB/S2/RJN-051/2015) for financial support. We thank computing facilities at MonARCH cluster, Monash University.

Appendix A: Model non-dimensionalization

The mechanical energy function and the signalling kinetics equations are non-dimensionalized with characteristic time scale $\frac{\eta}{\Gamma} = 1$ and characteristic length scale $L_c = 1$ (Fig.1a) (Table I).

We simulate a monolayer of tissue with periodic boundary and $\mathcal{N}$ number of cells (no cell divisions or apoptosis). The model is implemented in CHASTE [40] using the C++ libraries. The equation of motion is solved numerically using a simple forward Euler discretization. The signalling equations are solved using Runge-Kutta-Merson method. We choose the time step size $\Delta t = 0.01$ (sufficiently small) to maintain the numerical stability. The initial levels of Notch and Delta concentration are chosen randomly from uniform random number in (0,1) for each cell α.

Appendix B: Number of clusters and cluster size

The median number of clusters and the median cluster size is calculated for 400 cells and 1800 steady state time frames using the density-based spatial clustering (DBSCAN) algorithm [41]. The cell α is considered a Delta cell if the concentration of Delta molecule in the cell is greater than D_{critical}. A group of Delta cells is considered to be in dense region if minimum number of Delta cells in the cluster is 3. Two cells are considered to be touching each other if the Euclidean distance between both the cells are less than or equal to 1.5

Appendix C: Shape ratio

The shape ratio is calculated for 400 cells and 1800 steady state time frames. The cell α is considered a Delta cell if the concentration of Delta molecule in the cell is greater than D_{critical}. The inertia matrix of a single cluster is computed as follows:

$$\mathbf{A} = \begin{bmatrix} \mathbf{I}_{xx} & \mathbf{I}_{xy} \\ \mathbf{I}_{xy} & \mathbf{I}_{yy} \end{bmatrix}$$

$$\mathbf{I}_{xx} = \sum_{i=1}^{N_c} (A_i(\mathbf{x}_i - \mathbf{x}_{\text{mean}})^2), \tag{C1}$$

$$\mathbf{I}_{yy} = \sum_{i=1}^{N_c} (A_i(\mathbf{y}_i - \mathbf{y}_{\text{mean}})^2), \tag{C2}$$

$$\mathbf{I}_{xy} = \sum_{i=1}^{N_c} (A_i(\mathbf{x}_i - \mathbf{x}_{\text{mean}})(\mathbf{y}_i - \mathbf{y}_{\text{mean}})) \tag{C3}$$

where, N_c is the number of cells in a cluster. Eigen values of $\mathbf{A}$ is calculated and shape ratio is estimated as the ratio of the maximum and minimum eigen values. The median of the shape ratios of all the clusters of a time frame is calculated, and the median of all the shape ratios obtained from all time frames is the final shape ratio.

Appendix D: Movie captions

Movie-1 corresponding to Fig.2a. Signalling pattern formed by contact mediated signalling via junctional contacts $\frac{\beta_j}{\beta_p} = 99$.

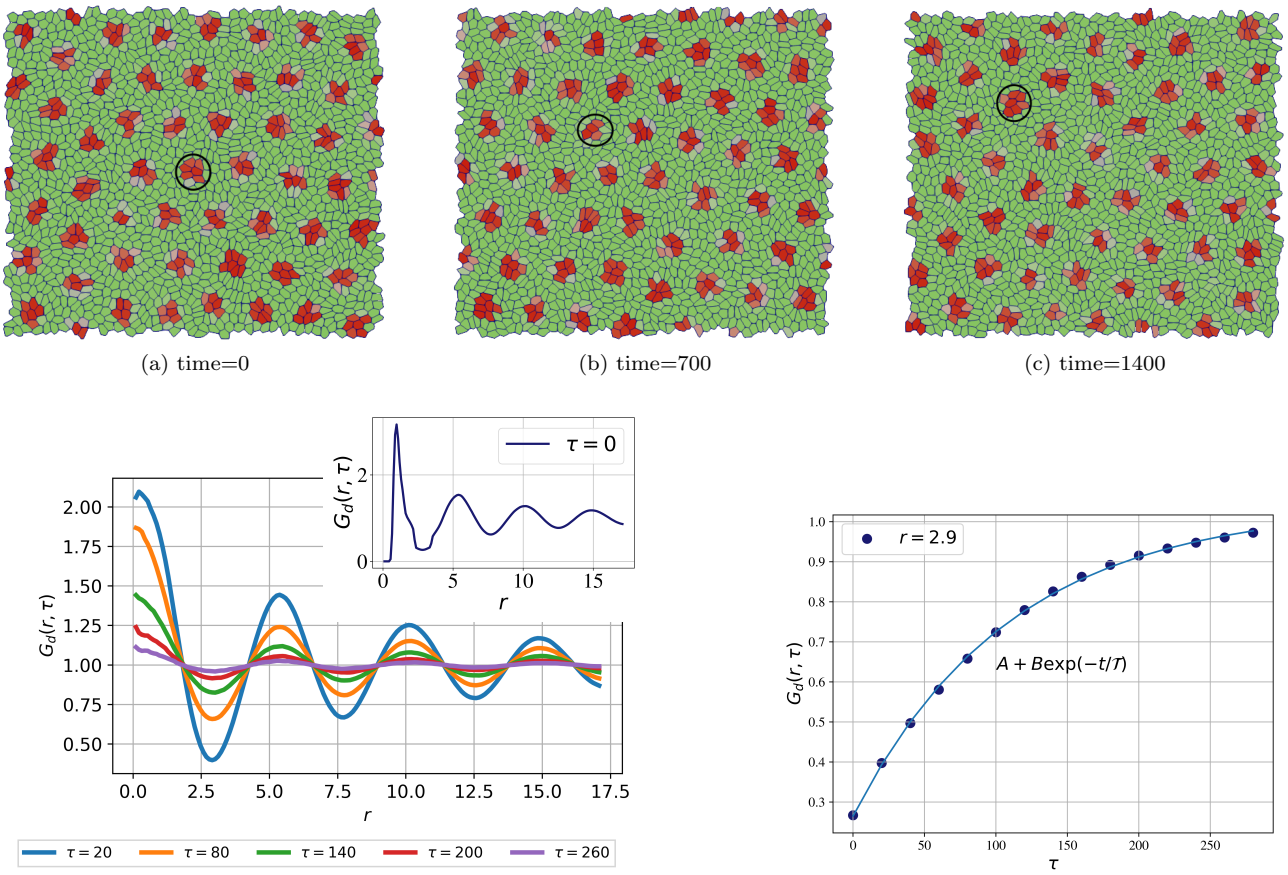

(a) time=0 (b) time=700 (c) time=1400

(d) (e)

FIG. 5. Screenshots and plots showing the effect of cell motility and tissue mechanics on Delta-Notch pattern formation. The parameters used for the simulations are $R_N = R_D = \rho = \mu = 10$, $\Lambda = -14.32$, $D_r = 0.001$, $\xi = 0$, $\Delta\theta = \pi/2$, $T = 0.1$ and $v_0 = 0.31$. The shape parameter for the cells $p_0 > 3.82$, the so called fluidisation threshold. (a)-(c) The spot-like Delta patterns keep re-arranging in space as a function of time. (d) Plot of the Delta-Delta correlation function $G_d(r,\tau)$ shows clear spatial pattern with a length scale of approximately 5 cell lengths. Although the shape of the function $G_d(r,\tau)$ does not change with τ, its amplitude decreases, thus indicating that the dynamic nature of the patterns. (e) The magnitude of $G(r,\tau)$ as a function of τ for $r \approx 2.9$ is plotted as a function of time. An exponentially saturating function of the form $A + B\exp(-t/\mathcal{T})$ fits well to these values with $\mathcal{T} \approx 100$ and provides the time-scale for pattern re-arrangement.

Movie-2 corresponding to Fig.3a. Pattern obtained using the model for $R_N = R_D = \rho = \mu = 1$, $D_r = 10^{-3}$, $\frac{\beta_j}{\beta_p} = 10^{-2}$, $\Delta\theta = \pi/4$, $v_0 = 3.1 \times 10^{-4}$, and $\Lambda = -13.77$ and $T = 0.1$.

Movie-3 corresponding to Fig.3b. Pattern obtained using the model for $R_N = R_D = \rho = \mu = 1$, $D_r = 10^{-3}$, $\frac{\beta_j}{\beta_p} = 10^{-2}$, $\Delta\theta = \pi/4$, $v_0 = 3.1 \times 10^{-4}$, and $\Lambda = -13.77$ and $T = 0.5$.

Movie-4 corresponding to Fig.3c. Pattern obtained using the model for $R_N = R_D = \rho = \mu = 1$, $D_r = 10^{-3}$, $\frac{\beta_j}{\beta_p} = 10^{-2}$, $\Delta\theta = \pi/4$, $v_0 = 3.1 \times 10^{-4}$, and $\Lambda = -13.77$ and $T = 0.6$.

Movie-5 corresponding to Fig.3d. Pattern obtained using the model for $R_N = R_D = \rho = \mu = 1$, $D_r = 10^{-3}$, $\frac{\beta_j}{\beta_p} = 10^{-2}$, $\Delta\theta = \pi/4$, $v_0 = 3.1 \times 10^{-4}$, and $\Lambda = -13.77$ and $T = 0.8$.

Movie-6 corresponding to Fig.3e. Pattern obtained using the model for $R_N = R_D = \rho = \mu = 1$, $D_r = 10^{-3}$, $\frac{\beta_j}{\beta_p} = 10^{-2}$, $\Delta\theta = \pi/4$, $v_0 = 3.1 \times 10^{-4}$, and $\Lambda = -13.77$ and $T = 0.9$.

Movie-7 corresponding to Fig.3f. Pattern obtained using the model for $R_N = R_D = \rho = \mu = 1$, $D_r = 10^{-3}$, $\frac{\beta_j}{\beta_p} = 10^{-2}$, $\Delta\theta = \pi/4$, $v_0 = 3.1 \times 10^{-4}$, and $\Lambda = -13.77$ and $T = 0.94$. **Movie-8** corresponding to Fig.4a. Pattern obtained using the model with parameter $R_N = R_D = \rho = \mu = 1$, $\Lambda = -13.77$, $D_r = 0.1$, $v_0 = 3.1 \times 10^{-4}$, $\frac{\beta_j}{\beta_p} = 0.01$, $T = 0.5$ and $\Delta\theta = \pi/4$ and $\xi/D_r = 0$.

Movie-9 corresponding to Fig.4b. Pattern obtained using the model with parameter $R_N = R_D = \rho = \mu = 1$, $\Lambda = -13.77$, $D_r = 0.1$, $v_0 = 3.1 \times 10^{-4}$, $\frac{\beta_j}{\beta_p} = 0.01$, $T = 0.5$ and $\Delta\theta = \pi/4$ and $\xi/D_r = 0.5$.

Movie-10 corresponding to Fig.4c. Pattern obtained using the model with parameter $R_N = R_D = \rho = \mu = 1$, $\Lambda = -13.77$, $D_r = 0.1$, $v_0 = 3.1 \times 10^{-4}$, $\frac{\beta_j}{\beta_p} = 0.01$, $T = 0.5$ and $\Delta\theta = \pi/4$ and $\xi/D_r = 1.0$.

Movie-11 corresponding to Fig.4d. Pattern obtained using the model with parameter $R_N = R_D = \rho = \mu = 1$, $\Lambda = -13.77$, $D_r = 0.1$, $v_0 = 3.1 \times 10^{-4}$, $\frac{\beta_j}{\beta_p} = 0.01$, $T = 0.5$ and $\Delta\theta = \pi/4$ and $\xi/D_r = 1.5$.

Movie-12 corresponding to Fig.4e. Pattern obtained using the model with parameter $R_N = R_D = \rho = \mu = 1$, $\Lambda = -13.77$, $D_r = 0.1$, $v_0 = 3.1 \times 10^{-4}$, $\frac{\beta_j}{\beta_p} = 0.01$, $T = 0.5$ and $\Delta\theta = \pi/4$ and $\xi/D_r = 2.0$.

Movie-13 corresponding to Fig.4f. Pattern obtained using the model with parameter $R_N = R_D = \rho = \mu = 1$, $\Lambda = -13.77$, $D_r = 0.1$, $v_0 = 3.1 \times 10^{-4}$, $\frac{\beta_j}{\beta_p} = 0.01$, $T = 0.5$ and $\Delta\theta = \pi/4$ and $\xi/D_r = 2.5$.

Movie-14 corresponding to Fig.5a-c. The parameter values used for the simulations are $R_N = R_D = \rho = \mu = 10$, $\frac{\beta_j}{\beta_p} = 0.01$, $\Lambda = -14.32$, $D_r = 0.001$, $\xi = 0$, $\Delta\theta = \pi/2$, $T = 0.1$ and $v_0 = 0.31$. The shape parameter for the cells $p_0 > 3.82$.

Movie-15 for the tissue in fluid region with stripe-like pattern. The parameter values used for the simulations are $R_N = R_D = \rho = \mu = 10$, $\frac{\beta_j}{\beta_p} = 0.01$, $\Lambda = -14.32$, $D_r = 0.1$, $\xi = 0.25$, $\Delta\theta = \pi/4$, $T = 0.5$ and $v_0 = 0.31$. The shape parameter for the cells $p_0 > 3.82$.

[1] P. Gross, K. V. Kumar, and S. W. Grill, How active mechanics and regulatory biochemistry combine to form patterns in development, Annual review of biophysics **46**, 337 (2017).

[2] M. Cohen, M. Georgiou, N. L. Stevenson, M. Miodownik, and B. Baum, Dynamic Filopodia Transmit Intermittent Delta-Notch Signaling to Drive Pattern Refinement during Lateral Inhibition, Developmental Cell **19**, 78 (2010).

[3] G. L. Hunter, Z. Hadjivasiliou, H. Bonin, L. He, N. Perrimon, G. Charras, and B. Baum, Coordinated control of Notch/Delta signalling and cell cycle progression drives lateral inhibition-mediated tissue patterning, Development **143**, 2305 (2016).

[4] D. S. Eom, E. J. Bain, L. B. Patterson, M. E. Grout, and D. M. Parichy, Long-distance communication by specialized cellular projections during pigment pattern development and evolution, eLife **4**, 1 (2015).

[5] H. Hamada, M. Watanabe, H. E. Lau, T. Nishida, T. Hasegawa, D. M. Parichy, and S. Kondo, Involvement of Delta/Notch signaling in zebrafish adult pigment stripe patterning, Development **141**, 318 (2014).

[6] G. Forgacs and S. A. Newman, *Biological physics of the developing embryo* (Cambridge University Press, 2005).

[7] K. Uriu, Y. Morishita, and Y. Iwasa, Random cell movement promotes synchronization of the segmentation clock, Proceedings of the National Academy of Sciences **107**, 4979 (2010).

[8] K. Uriu and L. G. Morelli, Article Collective Cell Movement Promotes Synchronization of Coupled Genetic Oscillators, Biophysj **107**, 514 (2014).

[9] A. M. Turing, The chemical basis of morphogenesis, Bulletin of mathematical biology **52**, 153 (1990).

[10] J. B. Green and J. Sharpe, Positional information and reaction-diffusion: two big ideas in developmental biology combine, Development **142**, 1203 (2015).

[11] M. Inaba, H. Yamanaka, and S. Kondo, Pigment pattern formation by contact-dependent depolarization, Science (New York, N.Y.) **335**, 677 (2012).

[12] T. B. Kornberg and S. Roy, Cytonemes as specialized signaling filopodia, Development **141**, 729 (2014).

[13] J. R. Collier, N. A. Monk, P. K. Maini, and J. H. Lewis, Pattern formation by lateral inhibition with feedback: A mathematical model of delta-notch intercellular signalling, Journal of Theoretical Biology **183**, 429 (1996), arXiv:0307072v1 [arXiv:quant-ph].

[14] F. Corson, L. Couturier, H. Rouault, K. Mazouni, and F. Schweisguth, Self-organized notch dynamics generate stereotyped sensory organ patterns in drosophila, Mechanisms of Development **145**, S10 (2017), 18th International Congress of Developmental Biology 18-22 June, University Cultural Centre, National University of Singapore.

[15] Z. Hadjivasiliou, G. L. Hunter, and B. Baum, A new mechanism for spatial pattern formation via lateral and protrusionmediated lateral signalling, Journal of the Royal Society Interface **13**, 10.1098/rsif.2016.0484 (2016).

[16] G. Vasilopoulos and K. J. Painter, Mathematical Biosciences Pattern formation in discrete cell tissues under long range filopodia-based direct cell to cell contact, Mathematical Biosciences **273**, 1 (2016).

[17] D. Sprinzak, A. Lakhanpal, L. Lebon, L. A. Santat, M. E. Fontes, G. A. Anderson, J. Garcia-Ojalvo, and M. B. Elowitz, Cis-interactions between Notch and Delta generate mutually exclusive signalling states, Nature **465**, 86 (2010).

[18] D. Sprinzak, A. Lakhanpal, L. LeBon, J. Garcia-Ojalvo, and M. B. Elowitz, Mutual inactivation of Notch receptors and ligands facilitates developmental patterning, PLoS Computational Biology **7**, 10.1371/journal.pcbi.1002069 (2011).

[19] S. Chigurupati, T. V. Arumugam, T. G. Son, J. D. Lathia, S. Jameel, M. R. Mughal, S.-C. Tang, D.-G. Jo, S. Camandola, M. Giunta, *et al.*, Involvement of notch signaling in wound healing, PloS one **2**, e1167 (2007).

[20] A. S. Ghabrial and M. A. Krasnow, Social interactions among epithelial cells during tracheal branching morphogenesis, Nature **441**, 746 (2006).

[21] G. Lebreton and J. Casanova, Specification of leading and trailing cell features during collective migration in the drosophila trachea, Journal of cell science **127**, 465 (2014).

[22] R. Riahi, J. Sun, S. Wang, M. Long, D. D. Zhang, and P. K. Wong, Notch1-Dll4 signalling and mechanical force regulate leader cell formation during collective cell migration, Nature Communications **6**, 1 (2015), arXiv:15334406.

[23] S. Lowell and F. M. Watt, Delta regulates keratinocyte spreading and motility independently of differentiation, Mechanisms of Development **107**, 133 (2001).

[24] W. R. Gordon, B. Zimmerman, L. He, L. J. Miles, J. Huang, K. Tiyanont, D. G. McArthur, J. C. Aster, N. Perrimon, J. J. Loparo, and S. C. Blacklow, Mechanical Allostery: Evidence for a Force Requirement in the Proteolytic Activation of Notch, Developmental Cell **33**, 729 (2015).

[25] L. Meloty-Kapella, B. Shergill, J. Kuon, E. Botvinick, and G. Weinmaster, Notch Ligand Endocytosis Generates Mechanical Pulling Force Dependent on Dynamin, Epsins, and Actin, Developmental Cell **22**, 1299 (2012).

[26] K. Uriu, S. Ares, A. C. Oates, and L. G. Morelli, Optimal cellular mobility for synchronization arising from the gradual recovery of intercellular interactions,

Physical Biology **9**, 036006 (2012).

[27] D. Bi, X. Yang, M. C. Marchetti, and M. L. Manning, Motility-driven glass and jamming transitions in biological tissues, Physical Review X **6**, 1 (2016), arXiv:1509.06578.

[28] R. Farhadifar, J. C. Röper, B. Aigouy, S. Eaton, and F. Jülicher, The Influence of Cell Mechanics, Cell-Cell Interactions, and Proliferation on Epithelial Packing, Current Biology **17**, 2095 (2007), arXiv:arXiv:1112.5905v1.

[29] D. Bi, J. H. Lopez, J. M. Schwarz, and M. L. Manning, A density-independent rigidity transition in biological tissues, Nature Physics **11**, 1074 (2015), arXiv:1409.0593.

[30] K. H. Nagai, Y. Sumino, R. Montagne, I. S. Aranson, and H. Chaté, Collective motion of self-propelled particles with memory, Phys. Rev. Lett. **114**, 168001 (2015).

[31] T. Vicsek, A. Czirók, E. Ben-Jacob, I. Cohen, and O. Shochet, Novel type of phase transition in a system of self-driven particles, Phys. Rev. Lett. **75**, 1226 (1995).

[32] A. Martín-Gómez, D. Levis, A. Díaz-Guilera, and I. Pagonabarraga, Collective motion of active brownian particles with polar alignment, Soft Matter **14**, 2610 (2018).

[33] D. M. Sussman, cellgpu: Massively parallel simulations of dynamic vertex models, Computer Physics Communications **219**, 400 (2017).

[34] D. Meyen, K. Tarbashevich, T. U. Banisch, C. Wittwer, M. Reichman-Fried, B. Maugis, C. Grimaldi, E.-M. Messerschmidt, and E. Raz, Dynamic filopodia are required for chemokine-dependent intracellular polarization during guided cell migration in vivo, Elife **4**, e05279 (2015).

[35] L. Capuana, A. Boström, and S. Etienne-Manneville, Multicellular scale front-to-rear polarity in collective migration, Current opinion in cell biology **62**, 114 (2020).

[36] N. Guisoni, R. Martinez-Corral, J. Garcia-Ojalvo, and J. de Navascués, Diversity of fate outcomes in cell pairs under lateral inhibition, Development **144**, 1177 (2017), https://dev.biologists.org/content/144/7/1177.full.pdf.

[37] O. Shaya, U. Binshtok, M. Hersch, D. Rivkin, S. Weinreb, L. Amir-Zilberstein, B. Khamaisi, O. Oppenheim, R. A. Desai, R. J. Goodyear, G. P. Richardson, C. S. Chen, and D. Sprinzak, Cell-Cell Contact Area Affects Notch Signaling and Notch-Dependent Patterning, Developmental Cell **40**, 505 (2017).

[38] D. Henrique and F. Schweisguth, Mechanisms of notch signaling: a simple logic deployed in time and space, Development **146**, 10.1242/dev.172148 (2019).

[39] D. B. Staple, R. Farhadifar, J.-C. Röper, B. Aigouy, S. Eaton, and F. Jülicher, Mechanics and remodelling of cell packings in epithelia, The European Physical Journal E **33**, 117 (2010).

[40] G. R. Mirams, C. J. Arthurs, M. O. Bernabeu, R. Bordas, J. Cooper, A. Corrias, Y. Davit, S.-J. Dunn, A. G. Fletcher, D. G. Harvey, *et al.*, Chaste: an open source c++ library for computational physiology and biology, PLoS Comput Biol **9**, e1002970 (2013).

[41] M. Ester, H. P. Kriegel, J. Sander, and X. Xu, Proceedings of the second international conference on knowledge discovery and data mining (kdd-96) (1996).